Developmental Cell
Short Article

A Calcium Dialog Mediated by the *FERONIA* Signal Transduction Pathway Controls Plant Sperm Delivery

Quy A. Ngo,[1,*] Hannes Vogler,[1] Dmytro S. Lituiev,[1] Anna Nestorova,[1] and Ueli Grossniklaus[1,*]
[1]Institute of Plant Biology and Zürich-Basel Plant Science Center, University of Zürich, Zollikerstrasse 107, 8008 Zürich, Switzerland
*Correspondence: qango@access.uzh.ch (Q.A.N.), grossnik@botinst.uzh.ch (U.G.)
http://dx.doi.org/10.1016/j.devcel.2014.04.008

SUMMARY

Sperm delivery for double fertilization of flowering plants relies on interactions between the pollen tube (PT) and two synergids, leading to programmed cell death (PCD) of the PT and one synergid. The mechanisms underlying the communication among these cells during PT reception is unknown. We discovered that the synergids control this process by coordinating their distinct calcium signatures in response to the calcium dynamics and growth behavior of the PT. Induced and spontaneous aberrant calcium responses in the synergids abolish the two coordinated PCD events. Components of the *FERONIA* (*FER*) signaling pathway are required for initiating and modulating these calcium responses and for coupling the PCD events. Intriguingly, the calcium signatures are interchangeable between the two synergids, implying that their fates of death and survival are determined by reversible interactions with the PT. Thus, complex intercellular interactions involving a receptor kinase pathway and calcium-mediated signaling control sperm delivery in plants.

INTRODUCTION

Unlike in animals, where motile sperm actively swim to fertilize the egg, plant sperm cells are delivered by the tip-growing pollen tube (PT; male gametophyte) to the embryo sac (female gametophyte), which consists of two gametes and several accessory cells, including the synergids (Nawaschin, 1898; Guignard, 1899). Successful PT reception relies on intercellular interactions between cells of the male and female gametophytes, the PT and synergids, respectively (Kessler and Grossniklaus, 2011). In *Arabidopsis thaliana*, after PT arrival, one of the two genetically identical synergids collapses as the PT ruptures to release the two sperm cells, which subsequently fertilize the two female gametes (Hamamura et al., 2011). These intercellular interactions were uncovered by the isolation of mutants affecting PT reception either specifically in the synergids (*fer/sirène*, Huck et al., 2003; Rotman et al., 2003; Escobar-Restrepo et al., 2007; *lorelei* [*lre*], Capron et al., 2008; and *nortia* [*nta*], Kessler et al., 2010), the PT (*myb97;myb101;myb120* triple mutant, Leydon et al., 2013; Liang et al., 2013), or both gametophytes (*abstinence by mutual consent*, Boisson-Dernier et al., 2008), suggesting that both are actively involved in this process. Static imaging analyses showed that in these mutants PTs fail to rupture but continue to grow inside the embryo sac, so that neither the PT nor the receptive synergid undergoes programmed cell death (PCD), and thus no sperm cells are delivered to effect double fertilization. Yet, the mechanisms underlying this intercellular communication remain poorly understood. Recently, dynamic changes in calcium levels have been observed during PT guidance and reception (Iwano et al., 2012), pointing to a possible link between the second messenger calcium and the sperm delivery process. However, how calcium signaling is triggered and what role it plays in these interactions is completely unknown. Furthermore, the calcium dynamics could be observed only in either the PT or the two superimposed synergids due to their spatial overlap, rendering the monitoring of intercellular interactions among these cells impossible. We aimed to resolve these issues by developing dynamic imaging techniques to determine whether the female gametophyte utilizes calcium signaling to direct PT reception. Using a multichannel live-imaging approach coupled with pharmacological studies and mutant analyses, we uncovered that the synergids control sperm delivery through the *FER* signal transduction pathway to initiate and modulate their distinct calcium signatures in response to the calcium dynamics and growth behavior of the PT. Our findings implicate that female control of sperm delivery in plants depends on highly coordinated calcium signaling among the interacting gametophytic cells.

RESULTS

The Two Synergids Orchestrate Their Calcium Dialogs with the Calcium Dynamics and Growth Behavior of the Pollen Tube

To distinguish real-time calcium dynamics in the three gametophytic cells, we oriented *Arabidopsis* ovules harboring these cells in a configuration that displayed two spatially nonoverlapping synergids (Figure 1A). We monitored cytosolic calcium levels ($[Ca^{2+}]_{cyt}$) of the synergids and PT simultaneously, using two genetically encoded calcium sensors of nonoverlapping emission spectra (Figure 1A; Experimental Procedures). The yellow cameleon (YC) 3.60 (Nagai et al., 2004) and R-GECO1 (Zhao et al., 2011) proteins were specifically expressed in the synergids and the PT under the *MYB98* (Kasahara et al., 2005) and *LAT52* (Twell et al., 1990) promoters, respectively (Figure 1A). We recorded the $[Ca^{2+}]_{cyt}$ dynamics at 5-s intervals throughout the entire PT reception process in living ovules, from the time the PT approached the micropylar pole of the synergids until

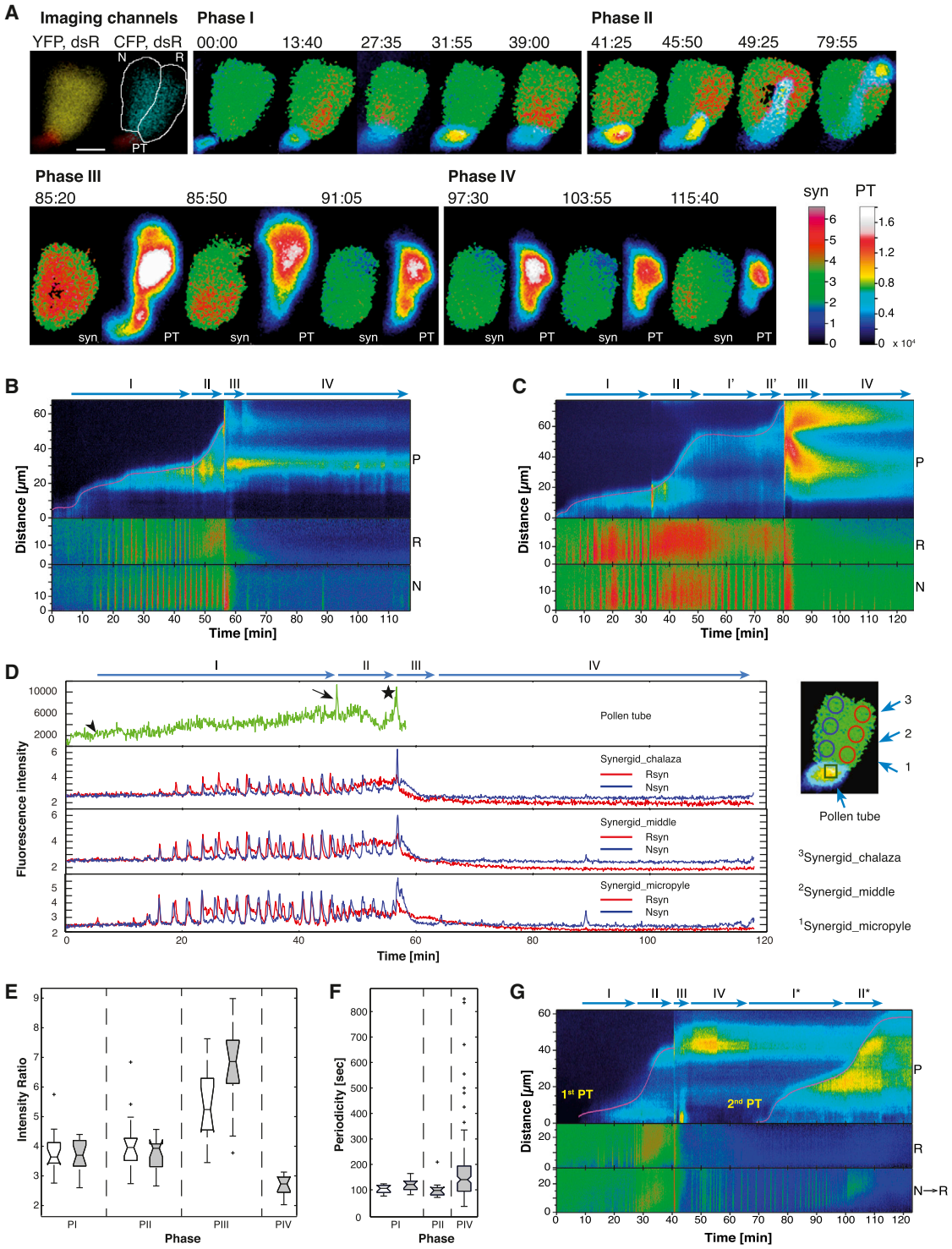

Figure 1. Highly Coordinated Calcium Dynamics during Pollen Tube Reception

(A) Snapshots of calcium imaging in the R-GECO1-expressing PT and YC3.60-expressing Rsyn (R) and Nsyn (N). First two images: fluorescence signals of imaging channels for YC3.60 (YFP, CFP) and R-GECO1 (dsR). Remaining images: time course of signal intensity ratio and raw signal intensity of calcium for synergids (syn) and PT, respectively. Phases I and II: superimposed calcium images of synergids and PT. Phases III and IV: separated calcium images of synergids (syn) and PT. Scale bar represents 10 μm.

(B, C, and G) Stacked kymographs of the PT (P), Rsyn (R), and Nsyn (N) calcium imaging. PT kymographs: the magenta line shows the PT tip growth path; the y-axis depicts the traveling distance of the PT tip from its arrival (bottom) until its rupture or stop (top). Synergid kymographs: calcium waves travel from the

(legend continued on next page)

30–60 min after the PT tip ruptured (Figure 1A; Movies S1A and S1B available online). To follow and compare dynamic $[Ca^{2+}]_{cyt}$ changes in the receptive synergid (Rsyn), nonreceptive synergid (Nsyn), and the PT simultaneously in space and time, we converted the three-dimensional (two-dimensional plus time) movies into stacked kymographs with two different false color scales for $[Ca^{2+}]_{cyt}$ in these cells (Figures 1B, 1C, and 1G). In all experiments (n = 13), we observed a striking common pattern of calcium dynamics among these three interacting cells with the following four phases:

Phase I—"slow PT growth"—lasted 34 (±15) min after the PT arrived at the micropylar pole of the Rsyn, as the PT grew slowly (0.5 ± 0.16 μm/min) along the micropylar region of the two synergids (Movies S1A and S1B). The first visible response of the synergids to PT arrival was that calcium spikes initiated at this end of the synergids and propagated as waves toward their chalazal poles at approximately 1–1.5 μm/sec (Figures 1A and 1B; Movie S1A). The magnitude of synergid $[Ca^{2+}]_{cyt}$, expressed as the YFP/CFP signal intensity ratio of YC3.60, rose from the basal level of about 2.1 (±0.5) before PT arrival to 3.7 (±0.6) and 3.8 (±0.7) in the Rsyn and the Nsyn, respectively (Figures 1D and 1E). The calcium oscillations were not synchronous in the two synergids (Figures 1A and 1B; Movie S1A), with the median period in the Rsyn being shorter than that in the Nsyn (106 s versus 121 s; Figure 1F). In contrast, $[Ca^{2+}]_{cyt}$ in the PT oscillated only locally with small fluctuations at its growing tip (Figures 1A and 1D; Movie S1A).

Phase II—"fast PT growth"—lasted 20 (±17) min. Upon an elevation of $[Ca^{2+}]_{cyt}$ at the PT tip to about four times the level it had at the time the first calcium spike occurred in the synergids (Figure 1D), the PT accelerated its growth three times (1.6 ± 0.7 μm/min) and grew across the Rsyn toward its chalazal pole (Figures 1A and 1B; Movie S1A). This high $[Ca^{2+}]_{cyt}$ was maintained for the first third of phase II, then subdued to the basal level, but increased again during the last quarter of phase II with occasional oscillations of pronouncedly high amplitudes (Figure 1B). Notably, within 1–3 min after the change in calcium and growth dynamics had initiated in the PT, calcium dynamics in the synergids were also altered: In the Nsyn, calcium waves continued to oscillate with a similar magnitude of 3.9 (±0.5) as in phase I (Figures 1D and 1E), but faster with a median period of 98 s (Figure 1F). In the Rsyn, the calcium oscillations were followed by a global spread of calcium that flooded the entire cell and was maintained throughout the entire phase II, reaching a magnitude of 4.0 (±1.0; Figures 1D and 1E), which was often highest at the chalazal pole (Figure 1B).

In three cases, once the PT had reached the chalazal pole of the synergids, it stopped growing for 24 (±4) min and then resumed its fast growth—but growing back toward the micropyle—for 5 (±2.4) min (Figure 1C; Movie S1B). The PT calcium dynamics during this period mimicked that of a shortened phase I and phase II (indicated as phase I′ and phase II′; Figure 1C). Unfailingly, the calcium oscillations were followed by the calcium flooding in the Rsyn as observed in the main phase II, albeit with a lower $[Ca^{2+}]_{cyt}$ magnitude (Figure 1C; Movie S1B). Therefore, this faithful switch in calcium dynamics of the Rsyn in response to the change in $[Ca^{2+}]_{cyt}$ and growth behavior of the PT underscores its physiological interaction with the PT and distinguishes the Rsyn from its genetically identical sister cell, the Nsyn. The two distinctive calcium signatures of the Rsyn and Nsyn suggest that different pathways might be activated in each cell, consistent with their destiny of death and survival, respectively.

Phase III—"PCDs"—was featured by the rupture of the PT tip and the collapse of the Rsyn (Figure 1A), with $[Ca^{2+}]_{cyt}$ at the PT tip increasing up to eight times compared to the level it had at the time of the first calcium spike in the synergids (Figures 1A and 1D). Within 5–10 s of PT rupture, $[Ca^{2+}]_{cyt}$ magnitudes in the Rsyn and Nsyn reached a maximum of 5.4 (±1.4) and 6.7 (±1.4) at their chalazal poles, respectively (Figures 1D and 1E), followed by the collapse of the Rsyn (Figure 1A). Although $[Ca^{2+}]_{cyt}$ in the Nsyn was significantly higher than in the Rsyn at this time (Figure 1E), the former's viability was not affected. Instead, $[Ca^{2+}]_{cyt}$ in the Nsyn subsided to the basal level within 2 min and remained at this level for 5.6 (±2.8) min without oscillations (Figures 1B–1D), manifesting a robust mechanism for regulating calcium homeostasis. These results also suggest that a prolonged high level, rather than a short burst of global $[Ca^{2+}]_{cyt,}$ could lead to PCD of the Rsyn, similar to other apoptosis or necrosis phenomena (Zhivotovsky and Orrenius, 2011). In contrast, a different mechanism, for instance a strong increase in turgor pressure, may underlie PT rupture (Benkert et al., 1997; Amien et al., 2010).

Phase IV—"oscillation recovery"—began with the resumption of calcium oscillations in the persistent synergid (former Nsyn) in the absence of a PT (Figures 1A–1D; Movies S1A and S1B). However, the magnitude of $[Ca^{2+}]_{cyt}$ reached only a modest level of 2.7 (±0.3; Figure 1E), and the periodicity was longer and more irregular (mean 166 ± 125 s, median 140 s; Figure 1F) than in phases I and II. Lasting for at least 60 min, the calcium oscillations during phase IV could be involved in functions of the persistent synergid after the PCD of the PT and Rsyn, for instance in repelling additional PTs once double fertilization has occurred, or in attracting further PTs if double fertilization failed (Beale et al., 2012; Kasahara et al., 2012; Maruyama et al., 2013; Völz et al., 2013). Indeed, in a rare case, we observed a second PT entering the embryo sac after the first PT had ruptured (Figure 1G; see also Movie S2). The persistent synergid at the end of phase IV now served as the new Rsyn, and its calcium signature resembled that of the original Rsyn, i.e., oscillations that were followed by a spread of calcium flooding the cell in response to alterations in the calcium dynamics and growth behavior of the PT (indicated as phase I* and II* in Figure 1G). This observation suggests that both synergids are inherently competent to activate the calcium signature correlated with the PCD pathway, depending on their specific communication with the PT.

micropylar pole (bottom) to the chalazal pole (top). Color scales represent calcium level in synergids and PT. (B) Four distinct phases of PT reception. (C) Additional phases I′ and II′ of PT growth. (G) Second PT arrived (at ~70 min) with growth phases indicated as I* and II* after the first PT ruptured.
(D) Calcium traces of ROIs in PT and synergids. Arrowhead: PT arrives; Arrow: PT accelerates; star: PT ruptures.
(E) $[Ca^{2+}]_{cyt}$ magnitude and (F) calcium oscillation periodicity of Rsyn (white box) and Nsyn (gray box) in different phases. P, phase. Middle line of box: median. Notch of box: 95% CI of the median.

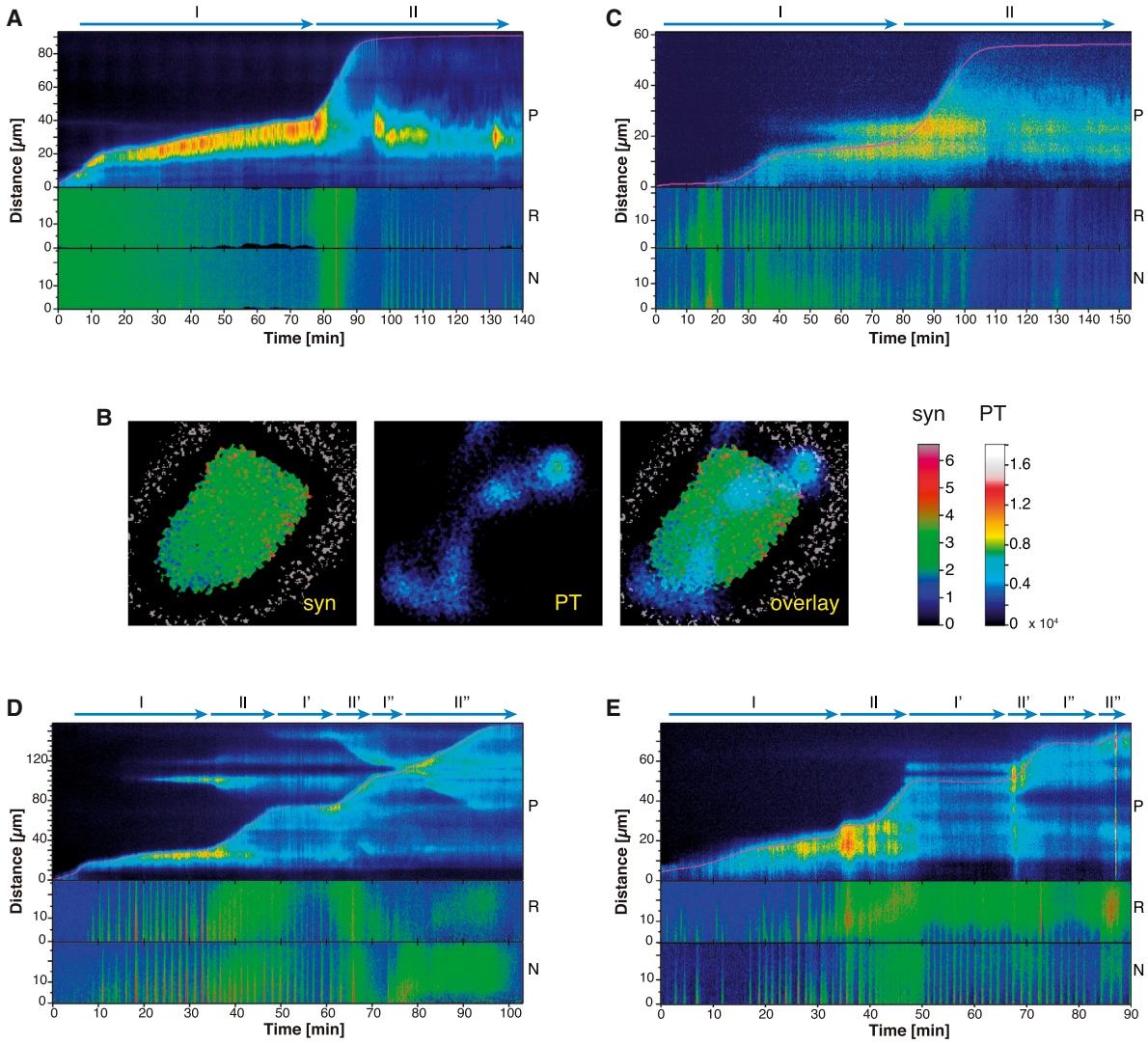

Figure 2. Disrupted Calcium Crosstalk during Aberrant Pollen Tube Reception

Stacked kymographs of aberrant calcium responses of WT synergids of flowers treated with 500 μM BAPTA-AM for 18 hr in (A) or without treatment in (C, D, and E). P, PT; R, Rsyn; N, Nsyn.

(B) Calcium images of spontaneous *fer*-like phenotype of WT synergids and PT at the end of phase II without PCD. Left: synergids; middle: PT; right: overlay of synergids and PT. Bottom: micropylar pole. Top: chalazal pole. Color scales represent calcium level in synergids and PT.

The Highly Coordinated Calcium Responses of the Synergids to the Pollen Tube Signals Are Essential for Sperm Delivery

To test whether the observed orchestrated calcium dynamics in the synergids, which were induced by the arriving PT, are required for PT reception, we used the intracellular calcium chelator BAPTA-AM (Kline and Kline, 1992) to deplete calcium in the synergids. In flowers treated with 500–600 μm BAPTA-AM (n = 5), the chelator abolished the initial calcium oscillations that occurred in response to PT arrival (Figure 2A). Subsequently, oscillations in phases I and II were reduced, and the PT did not rupture but continued to grow toward the central cell while the Rsyn remained alive (Figure 2A; see also Movie S3), as observed in the *fer*-class mutants (Kessler and Grossniklaus, 2011). Interestingly, even when the synergids were not treated with BAPTA-AM, both the PT and the Rsyn occasionally failed to undergo PCD at the end of phase II (Figure 2B). Thus, we also examined the calcium dynamics among the PT and synergids in these *fer*-like wild-type (WTferL) ovules (n = 4; Figures 2C–2E). We found that although the PT calcium and growth rate dynamics were not affected, the calcium signatures in the two synergids no longer followed the PT-responding schemes observed in the WT (Figures 2C–2E for WTferL, compared to Figures 1B, 1C, and 1G for WT). In one case, instead of discrete oscillations, a massive calcium spike was prolonged for 3–6 min at the beginning of phase I, and the responsive flooding of the Rsyn with calcium lasted for the first half of phase II and faded during the second half (Figure 2C). In three other cases, either the flooding of the Rsyn with calcium trailed off in the second half of phase II (Figure 2D), or the oscillation periods were excessively long at

the beginning of phase I (195–290 s; Figure 2E). These results indicate that disturbance in any feature of the dynamic and highly structured calcium signatures correlates with failed PCD. These features include (1) timely responsive oscillations in both synergids upon PT arrival, (2) timely responsive switch from oscillations to global calcium flood in the Rsyn upon PT acceleration, (3) accurate oscillation periodicity, and (4) sufficient calcium level and duration of the global calcium flood in the Rsyn. Thus, calcium *per se* or just a simple increase in the calcium level in the synergid is not sufficient to induce PCD. Rather, the sequence of highly coordinated and dynamic calcium responses—either in part or entirety—seems more relevant.

The *FERONIA* Pathway Is Required for Coordinated Calcium Responses in the Synergids and the Coupling of the Programmed Cell Death Events of the Receptive Synergid and Pollen Tube

Because both the female gametophytically active genes *FER*, *LRE*, *NTA*, and the elaborated calcium responses of the synergids to PT signals are necessary for sperm delivery, we investigated the role(s) of these genes in the calcium patterns observed during PT reception. We monitored calcium dynamics in all three mutants *fer*, *lre*, and *nta*, which disrupt normal PT reception and often attract multiple PTs (Huck et al., 2003; Rotman et al., 2003; Escobar-Restrepo et al., 2007; Capron et al., 2008; Kessler et al., 2010). The *fer* (n = 17) and *lre* (n = 14) mutant synergids displayed a range of aberrant calcium patterns, despite them being approached by WT PTs with normal calcium dynamics and growth kinetics (Figures 3A–3D): (1) completely abolished or barely detectable calcium spikes, regardless of the number of WT PTs received by the mutant embryo sac (Figure 3A; see also Movie S4), (2) sporadic calcium oscillations in both synergids without calcium flooding in the Rsyn during phase II (Figure 3B), and (3) delayed calcium flooding in the Rsyn during phase II, with or without $[Ca^{2+}]_{cyt}$ oscillations elsewhere (Figures 3C and 3D). In all cases, the $[Ca^{2+}]_{cyt}$ magnitudes in both synergids reached maximally 2.5 (±0.2) during the entire process, significantly lower than the value of 3.7–4.0 in WT. These results suggest that both *FER* and *LRE* are required not only for initiating the calcium oscillations in the synergids, but also for accurate responses to changes in PT calcium dynamics, presumably by perceiving or transducing signals from the PT to activate two distinct calcium signatures in the Rsyn and Nsyn. Notably, in one third of all cases during phase I or at the beginning of phase II, the PT grew backward over the Nsyn before growing forward to the chalazal pole (Figures 3E and 3F; see also Movie S5). This indicates that the *FER*- and *LRE*-dependent calcium signatures in the synergids could be involved in directing PT growth during this phase of PT reception.

In *nta* mutants (n = 11), we observed two types of aberrant calcium patterns and responses in the synergids: (1) a fade-off in the global calcium that flooded the Rsyn in the second half of phase II (Figure 3G), and (2) low $[Ca^{2+}]_{cyt}$ magnitudes (~3 ± 0.6; Figures 4A and 4B). Thus, unlike *FER* and *LRE*, *NTA* is not required to initiate calcium oscillations in the synergids but rather it is a modulator of the magnitude of the calcium signatures in the cells involved in PT reception. This is consistent with the fact that NTA has a calmodulin-binding domain (Kessler et al., 2010), and thus the amount of free cytosolic calcium in the synergids will be affected when the assumed calmodulin-NTA interactions are disturbed by the absence of NTA in the mutant. Infrequently, we noticed an uncoupling between the PCDs of the Rsyn and the PT in *nta* ovules, with the former collapsing at the end of phase II without the latter rupturing (two cases, Figure 3H; see also Movie S6), or vice versa (one case, Figure 3I; see also Movie S7). This finding suggests that *NTA* is also involved in coupling these two PCD events, which are not necessarily mutually dependent on each other.

Due to the incomplete penetrance of the *nta* phenotype, 80% of mutant ovules develop into fertilized seeds because of successful sperm delivery and double fertilization (Kessler et al., 2010). Indeed, in these WT-looking *nta* ovules (*nta*PTb; n = 5), we observed WT-like calcium dynamics with $[Ca^{2+}]_{cyt}$ magnitudes in phases I and II similar to those of WT (Figure 4), further strengthening the tight correlation between synergid calcium responses and the cellular dynamics of synergid-PT interactions.

Intriguingly, in a case where the PT did not stop at the chalazal pole of the Rsyn but grew backward to the micropyle and then across to the Nsyn, the two synergids switched their calcium signatures as the Nsyn now became the new Rsyn (Figure 3J; see also Movie S8). A similar switch occurred in the case where the PCDs of PT and Rsyn were uncoupled, where each synergid successively received a PT (Figure 3I; Movie S7). Together with the WT embryo sac that received two PTs (Figure 1G; Movie S2), these two *nta* cases support the idea that the two synergids could be in constant communication: the decision to activate the calcium signature for cell death (Rsyn) or cell survival (Nsyn) remains flexible during PT reception to respond to signals from the PT as its growth accelerates. Alternatively, stopping the information flow from the PT to the synergid that is not physically associated with it during acceleration might be responsible for the reversion from the Rsyn to Nsyn calcium signature.

DISCUSSION

The live-imaging approach of our study has unfolded multiple cellular and physiological events of the plant sperm delivery process, providing deeper understandings of not only the PT tip growth dynamics during PT reception but also how the synergid cells use calcium to control this course. Contrary to the long-mistaken view based on static microscopic images of prior studies that PT tip arrests growth inside the micropylar pole of the Rsyn and then ruptures to release sperm cells, our results reveal a nonconstant PT tip growth rate, with tip rupture occurring during the second phase of fast PT growth. Thus, unlike other tip-growing cells, such as plant root hairs or neuronal axons, where the terminal phenotype is tip growth arrest, the PT's terminal phenotype is PCD. Consequently, mutants defective in PT PCD display the continuous tip growth phenotype, which was interpreted in previous studies as a failure of the mutants to arrest PT growth (reviewed in Kessler and Grossniklaus, 2011). Our live-imaging evidence counters this theory because PT tip growth of the mutants *fer*, *lre*, and *nta* during the first slow growth phase was not faster than that of WT. Instead, the role of these three genes is consistent with effecting PCD of the PT and the Rsyn via calcium signaling. It is the temporal and spatial calcium dynamics highly structured in the two synergids in prompt response to PT signals that underlies these PCD

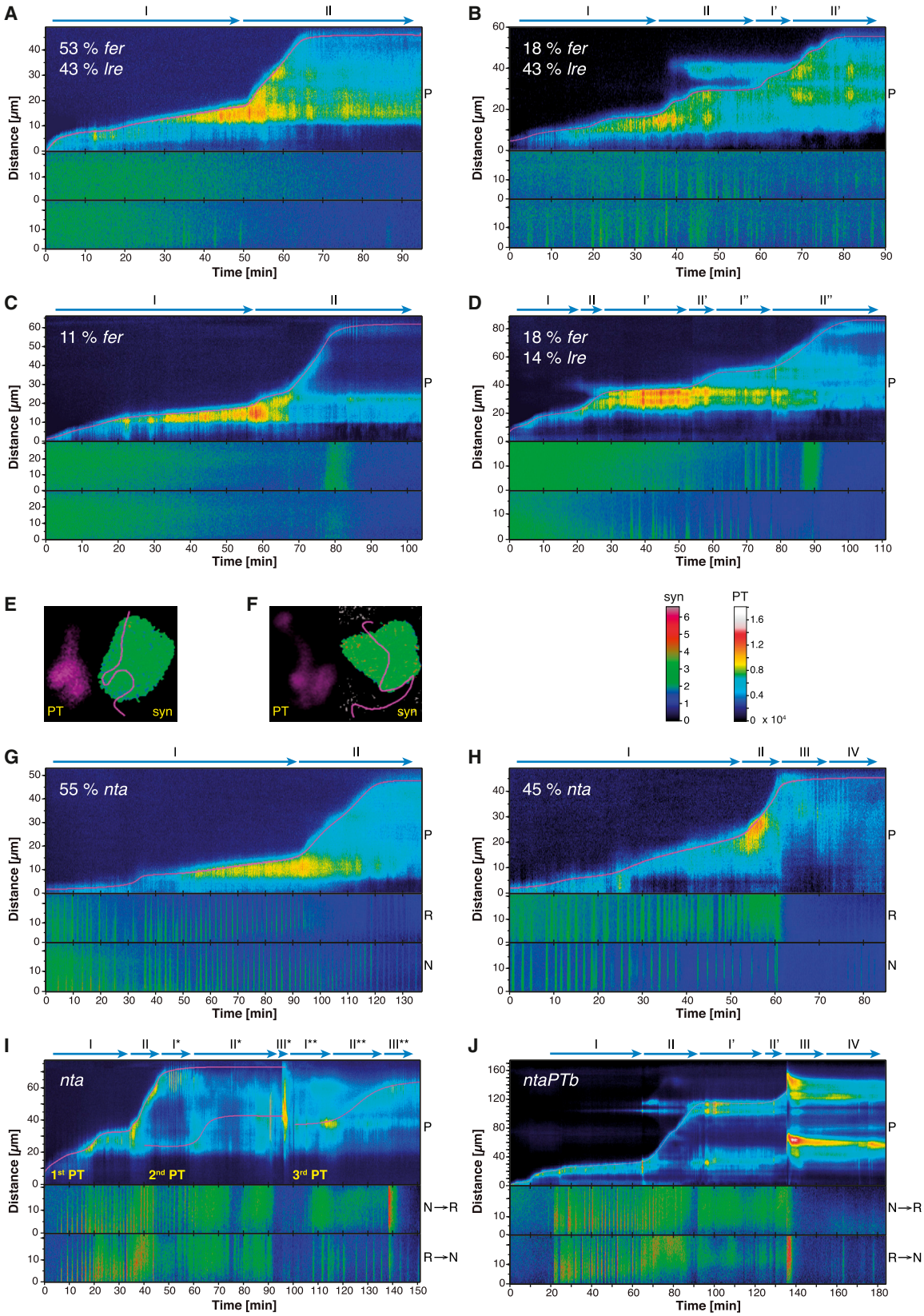

(legend on next page)

events. Furthermore, the absence of this responsive calcium dynamics in many *fer* and *lre* synergids despite having PT physical contact indicates that factors other than mechanical stimulus, such as ligand-receptor interactions between the PT and synergids, induce the synergid calcium responses. Altogether, our results suggest that active intercellular communications among the PT and two synergids coordinate their intracellular calcium dynamics mediated by the *FER* signaling pathway throughout PT reception.

Integrating the sequence of all observed cellular events with their associated distinctive physiological phenomena at each phase of sperm delivery, our study provides a conceptual framework for further dissecting the molecular mechanism of this multistep process. We speculate that (1) The receptor-like kinase FER collaborates with the GPI-anchored LRE at the synergid cell surface to (a) receive the arrival signals of the PT during its initial slow growth phase at the embryo sac entrance, and (b) translate the signals into the trigger of the calcium signaling cascade in the synergids in the form of calcium oscillations. (2) This cascade produces the synergid feedback signals to (a) instruct the PT directional tip growth for its acceleration during the next fast growth phase, and (b) repel additional PTs from entering the embryo sac. (3) The calcium burst in the PT tip at the start of its speeding phase serves as a new cue to the synergid physically associated with it, i.e., the Rsyn. In turn, the Rsyn responds by changing its calcium signature from oscillations to a sustained global calcium flood leading to its own PCD. This new calcium pattern of the Rsyn also generates a new feedback signal, similar to the maize ZmES4 peptide (Amien et al., 2010), for example, to set off PT tip rupture. The calmodulin-binding NTA modulates the intensity of the synergid calcium signatures with a more pronounced effect in the Rsyn during the global calcium flood, thus coordinating both PCD events. (4) The persistent synergid either retains its Nsyn calcium signature to repel additional PTs after successful double fertilization or re-programs its calcium signature to that of the Rsyn upon the arrival of new PTs for rescuing a failed fertilization event. This physiological plasticity not only renders a biomarker differentiating the two genetically and morphologically indistinguishable synergids but also signifies that the "PT receptivity" of the chosen synergid is not defined before PT arrival but at a later time during PT-synergid interactions.

The long-lasting (~55–90 min) dynamic calcium changes during PT reception suggest that many calcium-regulated proteins besides FER, LRE, and NTA participate in this three-way crosstalk, possibly generating a complex regulatory network. Recently, ethylene and reactive oxygen species have been implicated in PCD during PT reception (Völz et al., 2013; Duan et al., 2014), which opens up the possibility that these signaling pathways intersect with calcium signaling. Future studies on putative secreted signals/ligands (Leydon et al., 2013; Haruta et al., 2014), known (Peiter et al., 2005; Frietsch et al., 2007; Michard et al., 2011) and as yet unidentified calcium channels and transducers (Dodd et al., 2010; Hashimoto and Kudla, 2011) in the PT and synergids will undoubtedly provide new insights into this intercellular dialog that determines cell death and survival, which is essential for sperm delivery and thus double fertilization.

EXPERIMENTAL PROCEDURES

Transgenic Plant Generation

The calcium sensors *YC3.60*, *R-GECO1* and the *MYB98* promoter were PCR-amplified from the plasmids pBI121-Act1::YC3.60, pTorPE-R-GECO1, and *Arabidopsis thaliana* (Landsberg *erecta*) leaf DNA, respectively, and cloned into the pMOA36 or pMOA34/pLAT52 vectors to obtain the binary constructs with pMYB98 driving YC3.60 and pLAT52 driving R-GECO1. *Agrobacterium tumefaciens* (GV3101) was used to shuttle these constructs into WT *Arabidopsis thaliana* plants (*Ler* for YC3.60, Columbia (Col) for R-GECO1) using the floral dip method (Clough and Bent, 1998). Transgenic plants were selected on MS plates containing 10 mg/l Basta for YC3.60 and 50 mg/L Kanamycin for R-GECO1. Plants were grown at 22°C/18°C with a 16 hr light/8 hr dark cycle at 60% relative humidity on soil (ED73, Universalerde, Germany). Stable transgenic YC3.60 plants were crossed with the *fer* (*Ler*), *lre-3* (Col), and *nta* (Ws) mutants. Double homozygotes for YC3.60 and mutant alleles were selected by phenotyping the F2-F5 progeny for the presence of YFP/CFP fluorescence in the synergids and genotyping for the presence of mutant alleles by PCR. All PCR primer sequences are available upon request.

Microscopy

The ex vivo setup for fertilization was modified from Palanivelu and Preuss (2006). Dissected carpels *cum* ovules of emasculated flowers expressing YC3.60 were placed on the pollen germination culture medium (Boavida and McCormick, 2007). Stigmas of the flowers from *dde-2/dde-2* plants (von Malek et al., 2002) were pollinated with pollen expressing R-GECO1, excised 30 min later, and placed 150 μm away from the ovules. For calcium depletion experiments, emasculated flowers were floated in 500 μM BAPTA-AM (Santa Cruz Biotech, California, USA) for 17–22 hr before the carpels were dissected.

Time-lapse experiments were started after the PT had entered the ovule's micropyle inside the sample chamber maintained at 22°C and 92% relative humidity, using an Olympus IX81-ZDC2 wide-field inverted microscope with a 60× silicon oil objective (WD = 0.3 mm, NA = 1.3) and a CFP/YFP/DsRED filter set with single band exciters (436/10×, 580/20×) and emitters (465/25 m, 535/30 m, 630/60 m), at 5-s intervals with 10 ms of R-GECO1 and 2 × 30 ms of YC3.60 excitation. Signals were detected by a Hamamatsu EM-CCD camera C-9100 (30 ms per channel at 512 × 512 pixels) via the Olympus software xcellence-rt.

Image Processing

Raw time-lapse image stacks were drift-corrected by StackReg (Thévenaz et al., 1998) and MultiStackReg (http://bradbusse.net/downloads.html). $[Ca^{2+}]_{cyt}$ magnitudes in the synergids were calculated from the YFP/CFP signal intensities of 5 μm-diameter regions of interest (ROIs; Figure 1D) with various ImageJ Stack plugins (http://rsbweb.nih.gov/ij/index.html). The brightest signal intensity in a 4 × 4 μm ROI at the PT tip (Figure 1D) was tracked by Fiji's MTrackJ (Meijering et al., 2012) with the bright centroid method. The kymographs of the PT path and synergids were produced by ImageJ's Reslice

Figure 3. The *FERONIA* Pathway Is Required for Calcium Responses in Synergids and the Coupling of the Programmed Cell Death Events of the Receptive Synergid and Pollen Tube

Stacked kymographs of calcium imaging in *fer* and *lre* (A–D), *nta* (G–I), and a leaky *nta* mutant with normal PT reception (*ntaPTb*) (J). P, PT; R, Rsyn; N, Nsyn. Both synergids of *fer* and *lre* could receive PT (thus not designated as R or N). Color scale represents calcium level in synergids and PT. (H) Rsyn PCD without PT rupture in an *nta* mutant. (I) PT rupture without Rsyn PCD in an *nta* mutant. R → N: Rsyn at first PT arrival switching to Nsyn upon second PT arrival (at ~40 min). N → R: Nsyn at first PT arrival switching to Rsyn upon second PT arrival; this PT ruptured without Rsyn PCD (at ~95 min). (J) R →N: Rsyn switching to Nsyn (at ~65 min). N → R: Nsyn switching to Rsyn (at ~114 min). (E–F) Snap-shots of PT growth path in *lre* (E) and *fer* (F) mutants. Magenta image on the left of the PT and magenta line on the right of the synergids (syn) represent the PT growth path.

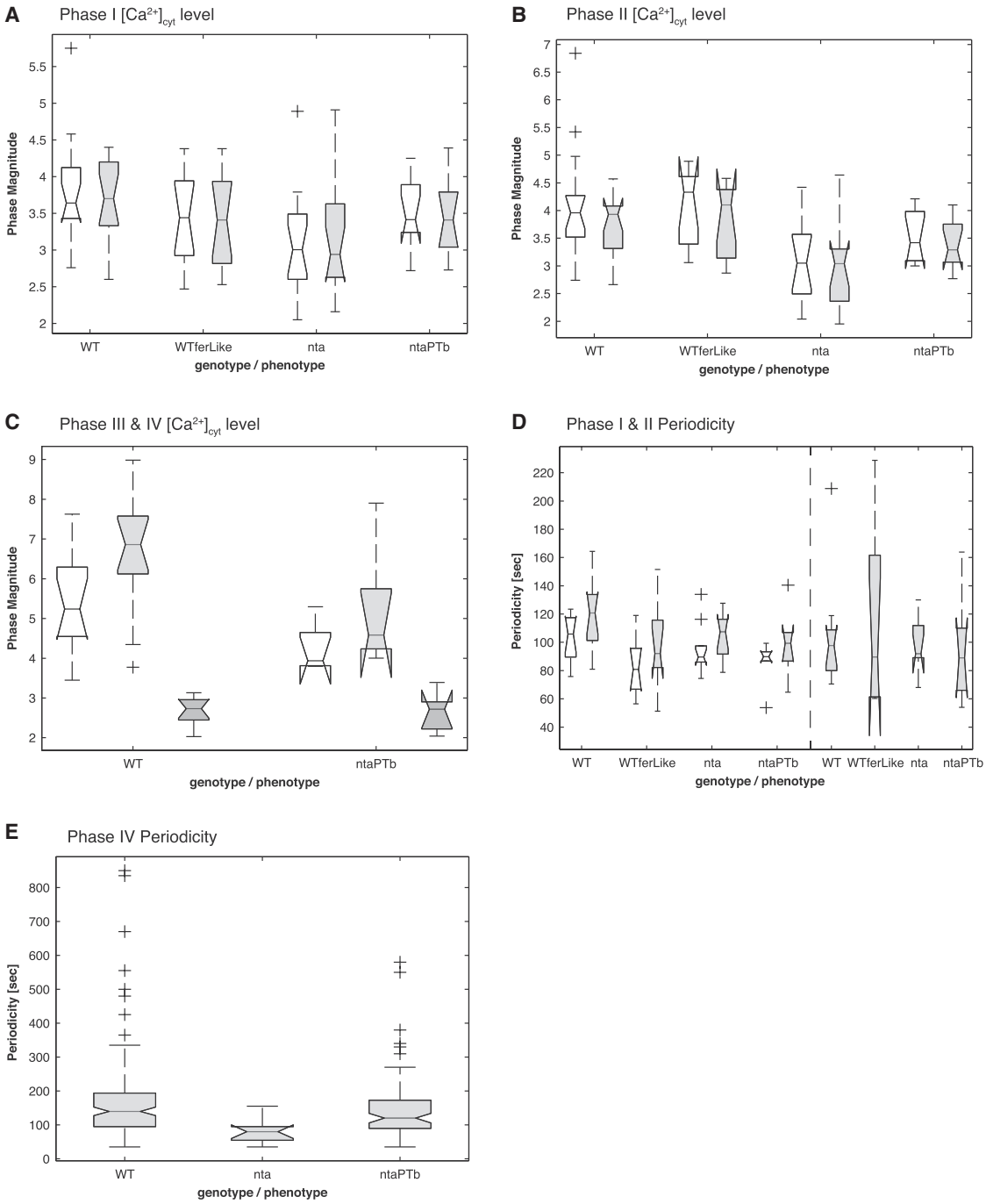

Figure 4. Magnitudes and Oscillations of Cytosolic Calcium in Synergids during Pollen Tube Reception

Calcium levels in phases I (A), II (B), III and IV (C), and oscillation periodicity in phases I, II (D), and IV (E). (D) Left of dashed line represents phase I; right of dashed line represents phase II. White box represents Rsyn, gray box represents Nsyn, dark gray box represents persistent synergid. WT, wild-type; WTferLike, *fer*-like WT; nta, *nortia*; ntaPTb, leaky *nta* mutant with successful PT reception.

function. MATLAB (Mathworks) was used to graph the calcium traces of the PT tip and synergids' ROIs and to stack the kymographs with distance and time axes. The highest synergid calcium magnitudes were calculated as the median of the 95th percentile of all signal intensity ratios for each phase. The periods of calcium wave oscillations in each phase were determined from counting the calcium peak numbers in the synergid kymographs. Notched box plots for calcium magnitudes and periods were generated by MATLAB. Calcium time-lapse movies (.avi) were produced by ImageJ at 15 frames/sec with JPEG compression.

SUPPLEMENTAL INFORMATION

Supplemental Information includes eight movies and can be found with this article online at http://dx.doi.org/10.1016/j.devcel.2014.04.008.

AUTHOR CONTRIBUTIONS

Q.A.N. and U.G. conceived the study; Q.A.N. designed the study and performed all experiments; Q.A.N. and H.V. processed and analyzed the data; D.S.L. processed part of the data; A.N. generated the transgenic lines expressing R-GECO1; U.G. provided materials, reagents, and means for data analysis; Q.A.N., H.V., and U.G. wrote the manuscript. All authors critically read and approved the manuscript for submission.

ACKNOWLEDGMENTS

We thank Venkatesan Sundaresan (University of California-Davis) for *lre* and Sharon Kessler (University of Zürich) for *nta* mutant seeds; Aurélien Boisson-Dernier (University of Zürich) and Markus Affolter (University of Basel) for helpful comments on the manuscript; Sharme Thirugnanarajah (University of Zürich) for genotyping *fer* plants, Arturo Bolaños, Valeria Gagliardini, Peter Kopf, and Daniela Guthörl (University of Zürich) for general lab support; and Urs Ziegler, Caroline Aemisegger, Christof Eichenberger (University of Zürich), and Jens Rietdof (Friedrich Miescher Institute Basel) for help and advice with microscopy. This project was supported by the University of Zürich, an International Research Fellowship (0754305) of the National Science Foundation (USA) to Q.A.N., an R'Equip and a project grant from the Swiss National Science Foundation to U.G., and an RTD project (PlantGrowth) and iPhD grant from SystemsX.ch to U.G.

Received: January 10, 2014
Revised: April 3, 2014
Accepted: April 7, 2014
Published: May 8, 2014

REFERENCES

Amien, S., Kliwer, I., Márton, M.L., Debener, T., Geiger, D., Becker, D., and Dresselhaus, T. (2010). Defensin-like ZmES4 mediates pollen tube burst in maize via opening of the potassium channel KZM1. PLoS Biol. *8*, e1000388.

Beale, K.M., Leydon, A.R., and Johnson, M.A. (2012). Gamete fusion is required to block multiple pollen tubes from entering an *Arabidopsis* ovule. Curr. Biol. *22*, 1090–1094.

Benkert, R., Obermeyer, G., and Bentrup, F.W. (1997). The turgor pressure of growing lily pollen tubes. Protoplasma *198*, 1–8.

Boavida, L.C., and McCormick, S. (2007). Temperature as a determinant factor for increased and reproducible in vitro pollen germination in *Arabidopsis thaliana*. Plant J. *52*, 570–582.

Boisson-Dernier, A., Frietsch, S., Kim, T.H., Dizon, M.B., and Schroeder, J.I. (2008). The peroxin loss-of-function mutation *abstinence by mutual consent* disrupts male-female gametophyte recognition. Curr. Biol. *18*, 63–68.

Capron, A., Gourgues, M., Neiva, L.S., Faure, J.E., Berger, F., Pagnussat, G., Krishnan, A., Alvarez-Mejia, C., Vielle-Calzada, J.P., Lee, Y.R., et al. (2008). Maternal control of male-gamete delivery in *Arabidopsis* involves a putative GPI-anchored protein encoded by the *LORELEI* gene. Plant Cell *20*, 3038–3049.

Clough, S.J., and Bent, A.F. (1998). Floral dip: a simplified method for *Agrobacterium*-mediated transformation of *Arabidopsis thaliana*. Plant J. *16*, 735–743.

Dodd, A.N., Kudla, J., and Sanders, D. (2010). The language of calcium signaling. Annu. Rev. Plant Biol. *61*, 593–620.

Duan, Q., Kita, D., Johnson, E.A., Aggarwal, M., Gates, L., Wu, H.M., and Cheung, A.Y. (2014). Reactive oxygen species mediate pollen tube rupture to release sperm for fertilization in *Arabidopsis*. Nat Commun *5*, 3129.

Escobar-Restrepo, J.M., Huck, N., Kessler, S., Gagliardini, V., Gheyselinck, J., Yang, W.C., and Grossniklaus, U. (2007). The *FERONIA* receptor-like kinase mediates male-female interactions during pollen tube reception. Science *317*, 656–660.

Frietsch, S., Wang, Y.F., Sladek, C., Poulsen, L.R., Romanowsky, S.M., Schroeder, J.I., and Harper, J.F. (2007). A cyclic nucleotide-gated channel is essential for polarized tip growth of pollen. Proc. Natl. Acad. Sci. USA *104*, 14531–14536.

Guignard, L. (1899). Sur les anthérozoides et la double copulation sexuelle chez les végétaux angiospermes. C R Acad Sci Paris *128*, 864–871.

Hamamura, Y., Saito, C., Awai, C., Kurihara, D., Miyawaki, A., Nakagawa, T., Kanaoka, M.M., Sasaki, N., Nakano, A., Berger, F., and Higashiyama, T. (2011). Live-cell imaging reveals the dynamics of two sperm cells during double fertilization in *Arabidopsis thaliana*. Curr. Biol. *21*, 497–502.

Haruta, M., Sabat, G., Stecker, K., Minkoff, B.B., and Sussman, M.R. (2014). A peptide hormone and its receptor protein kinase regulate plant cell expansion. Science *343*, 408–411.

Hashimoto, K., and Kudla, J. (2011). Calcium decoding mechanisms in plants. Biochimie *93*, 2054–2059.

Huck, N., Moore, J.M., Federer, M., and Grossniklaus, U. (2003). The *Arabidopsis* mutant *feronia* disrupts the female gametophytic control of pollen tube reception. Development *130*, 2149–2159.

Iwano, M., Ngo, Q.A., Entani, T., Shiba, H., Nagai, T., Miyawaki, A., Isogai, A., Grossniklaus, U., and Takayama, S. (2012). Cytoplasmic Ca^{2+} changes dynamically during the interaction of the pollen tube with synergid cells. Development *139*, 4202–4209.

Kasahara, R.D., Portereiko, M.F., Sandaklie-Nikolova, L., Rabiger, D.S., and Drews, G.N. (2005). *MYB98* is required for pollen tube guidance and synergid cell differentiation in *Arabidopsis*. Plant Cell *17*, 2981–2992.

Kasahara, R.D., Maruyama, D., Hamamura, Y., Sakakibara, T., Twell, D., and Higashiyama, T. (2012). Fertilization recovery after defective sperm cell release in *Arabidopsis*. Curr. Biol. *22*, 1084–1089.

Kessler, S.A., and Grossniklaus, U. (2011). She's the boss: signaling in pollen tube reception. Curr. Opin. Plant Biol. *14*, 622–627.

Kessler, S.A., Shimosato-Asano, H., Keinath, N.F., Wuest, S.E., Ingram, G., Panstruga, R., and Grossniklaus, U. (2010). Conserved molecular components for pollen tube reception and fungal invasion. Science *330*, 968–971.

Kline, D., and Kline, J.T. (1992). Repetitive calcium transients and the role of calcium in exocytosis and cell cycle activation in the mouse egg. Dev. Biol. *149*, 80–89.

Leydon, A.R., Beale, K.M., Woroniecka, K., Castner, E., Chen, J., Horgan, C., Palanivelu, R., and Johnson, M.A. (2013). Three *MYB* transcription factors control pollen tube differentiation required for sperm release. Curr. Biol. *23*, 1209–1214.

Liang, Y., Tan, Z.M., Zhu, L., Niu, Q.K., Zhou, J.J., Li, M., Chen, L.Q., Zhang, X.Q., and Ye, D. (2013). MYB97, MYB101 and MYB120 function as male factors that control pollen tube-synergid interaction in *Arabidopsis thaliana* fertilization. PLoS Genet. *9*, e1003933.

Maruyama, D., Hamamura, Y., Takeuchi, H., Susaki, D., Nishimaki, M., Kurihara, D., Kasahara, R.D., and Higashiyama, T. (2013). Independent control by each female gamete prevents the attraction of multiple pollen tubes. Dev. Cell *25*, 317–323.

Meijering, E., Dzyubachyk, O., and Smal, I. (2012). Methods for cell and particle tracking. Methods Enzymol. *504*, 183–200.

Michard, E., Lima, P.T., Borges, F., Silva, A.C., Portes, M.T., Carvalho, J.E., Gilliham, M., Liu, L.H., Obermeyer, G., and Feijó, J.A. (2011). Glutamate receptor-like genes form Ca^{2+} channels in pollen tubes and are regulated by pistil D-serine. Science *332*, 434–437.

Nagai, T., Yamada, S., Tominaga, T., Ichikawa, M., and Miyawaki, A. (2004). Expanded dynamic range of fluorescent indicators for $Ca^{(2+)}$ by circularly permuted yellow fluorescent proteins. Proc. Natl. Acad. Sci. USA *101*, 10554–10559.

Nawaschin, S. (1898). Resultate einer Revision der Befruchtungsvorgänge bei *Lilium martagon* und *Fritillaria tennela*. Bull. Acad. Imp. Sci. St. Petersbourg *9*, 377–382.

Palanivelu, R., and Preuss, D. (2006). Distinct short-range ovule signals attract or repel *Arabidopsis thaliana* pollen tubes in vitro. BMC Plant Biol. *6*, 7.

Peiter, E., Maathuis, F.J., Mills, L.N., Knight, H., Pelloux, J., Hetherington, A.M., and Sanders, D. (2005). The vacuolar Ca^{2+}-activated channel *TPC1* regulates germination and stomatal movement. Nature *434*, 404–408.

Rotman, N., Rozier, F., Boavida, L., Dumas, C., Berger, F., and Faure, J.E. (2003). Female control of male gamete delivery during fertilization in *Arabidopsis thaliana*. Curr. Biol. *13*, 432–436.

Thévenaz, P., Ruttimann, U.E., and Unser, M. (1998). A pyramid approach to subpixel registration based on intensity. IEEE Trans. Image Process. *7*, 27–41.

Twell, D., Yamaguchi, J., and McCormick, S. (1990). Pollen-specific gene expression in transgenic plants: coordinate regulation of two different tomato gene promoters during microsporogenesis. Development *109*, 705–713.

Völz, R., Heydlauff, J., Ripper, D., von Lyncker, L., and Groß-Hardt, R. (2013). Ethylene signaling is required for synergid degeneration and the establishment of a pollen tube block. Dev. Cell *25*, 310–316.

von Malek, B., van der Graaff, E., Schneitz, K., and Keller, B. (2002). The *Arabidopsis* male-sterile mutant *dde2-2* is defective in the *ALLENE OXIDE SYNTHASE* gene encoding one of the key enzymes of the jasmonic acid biosynthesis pathway. Planta *216*, 187–192.

Zhao, Y., Araki, S., Wu, J., Teramoto, T., Chang, Y.F., Nakano, M., Abdelfattah, A.S., Fujiwara, M., Ishihara, T., Nagai, T., and Campbell, R.E. (2011). An expanded palette of genetically encoded Ca^{2+} indicators. Science *333*, 1888–1891.

Zhivotovsky, B., and Orrenius, S. (2011). Calcium and cell death mechanisms: a perspective from the cell death community. Cell Calcium *50*, 211–221.